JACS
JOURNAL OF THE AMERICAN CHEMICAL SOCIETY
Article
pubs.acs.org/JACS

# Mixed Copper, Silver, and Gold Cyanides, $(M_xM'_{1-x})CN$: Tailoring Chain Structures To Influence Physical Properties

Ann M. Chippindale,*[,†] Simon J. Hibble,*[,‡] Edward J. Bilbé,[†] Elena Marelli,[†] Alex C. Hannon,[‡] Clémence Allain,[§] Robert Pansu,[§] and František Hartl*[,†]

[†]Department of Chemistry, University of Reading, Whiteknights, Reading RG6 6AD, U.K.
[‡]ISIS Facility, Rutherford Appleton Laboratory, Chilton, Didcot, Oxon OX11 0QX, U.K.
[§]PPSM, CNRS UMR 8531, Ecole Normale Supérieure de Cachan, 61, avenue du President Wilson, 94235 Cachan, France

Supporting Information

**ABSTRACT:** Binary mixed-metal variants of the one-dimensional MCN compounds (M = Cu, Ag, and Au) have been prepared and characterized using powder X-ray diffraction, vibrational spectroscopy, and total neutron diffraction. A solid solution with the AgCN structure exists in the $(Cu_xAg_{1-x})CN$ system over the range $(0 \le x \le 1)$. Line phases with compositions $(Cu_{1/2}Au_{1/2})CN$, $(Cu_{7/12}Au_{5/12})CN$, $(Cu_{2/3}Au_{1/3})CN$, and $(Ag_{1/2}Au_{1/2})CN$, all of which have the AuCN structure, are found in the gold-containing systems. Infrared and Raman spectroscopies show that complete ordering of the type $[M-C\equiv N-M'-N\equiv C-]_n$ occurs only in $(Cu_{1/2}Au_{1/2})CN$ and $(Ag_{1/2}Au_{1/2})CN$. The sense of the cyanide bonding was determined by total neutron diffraction to be $[Ag-NC-Au-CN-]_n$ in $(Ag_{1/2}Au_{1/2})CN$ and $[Cu-NC-Au-CN-]_n$ in $(Cu_{1/2}Au_{1/2})CN$. In contrast, in $(Cu_{0.50}Ag_{0.50})CN$, metal ordering is incomplete, and strict alternation of metals does not occur. However, there is a distinct preference (85%) for the N end of the cyanide ligand to be bonded to copper and for Ag−CN−Cu links to predominate. Contrary to expectation, aurophilic bonding does not appear to be the controlling factor which leads to $(Cu_{1/2}Au_{1/2})CN$ and $(Ag_{1/2}Au_{1/2})CN$ adopting the AuCN structure. The diffuse reflectance, photoluminescence, and 1-D negative thermal expansion (NTE) behaviors of all three systems are reported and compared with those of the parent cyanide compounds. The photophysical properties are strongly influenced both by the composition of the individual chains and by how such chains pack together. The NTE behavior is also controlled by structure type: the gold-containing mixed-metal cyanides with the AuCN structure show the smallest contraction along the chain length on heating.

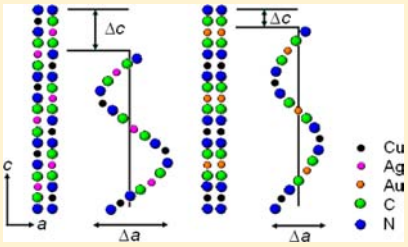


## INTRODUCTION

The copper, silver, and gold cyanides, CuCN, AgCN, and AuCN, all form structures containing infinite one-dimensional (1-D) chains of the form $[M-C\equiv N-]_n$.[1−5] The chains can be packed together in different ways to form 3-D solids. The simplest structure is adopted by AuCN, with linear $[Au-C\equiv N-]_n$ chains packed on a hexagonal lattice and the gold atoms arranged in layers (Figure 1a). In AgCN, the $[Ag-C\equiv N-]_n$ chains are also packed on a hexagonal lattice, but neighboring chains are displaced by ±one-third of the chain repeat distance along the *c* axis (Figure 1b). There is clearly a delicate balance of factors controlling which structure is adopted. The C≡N groups in neighboring chains are closer together in the AuCN structure than in the AgCN structure, and it might be expected that this would lead to increased repulsive interactions between the nonmetal atoms in AuCN compared to AgCN. It has been suggested that AuCN adopts its particular structure type because of favorable aurophilic interactions.[6] Copper cyanide forms a high-temperature phase, HT-CuCN, which also has the AgCN structure, suggesting that in the gold cyanide case there are additional factors, such as aurophilic interactions, that direct the structure to be AuCN type. A low-temperature form of CuCN, LT-CuCN, adopts a more complicated structure in which the $[Cu-C\equiv N-]_n$ chains form waves (Figure 2). In all these materials, there appears to be head-to-tail disorder of the cyanide groups, and the C and N atoms are therefore not distinguished in Figures 1 and 2.[7,8]

HT-CuCN, AgCN, and AuCN have interesting thermal behavior in that they all show 1-D negative thermal expansion (NTE) in the chain direction.[9] This can be envisioned as arising, at least in part, from dynamic wave motions of the chains of the type revealed in the static structure of LT-CuCN shown in Figure 2a. Other transverse motions of the atoms within the chains would also produce a contraction in the chain direction. We give a fuller account of possible motions in ref 9. It is notable that the magnitude of the NTE effect decreases by a factor of ~3.5 on going from HT-CuCN to AuCN.[9]

The photoluminescent behavior of the simple group 11 metal cyanides has been recently studied using UV light excitation.[10−12] Time-dependent density functional theory (TD-DFT) calculations on isolated chain fragments, $(M_n(CN)_{n+1})^-$ (M = Cu and $n$ = 1, 3, 5, 7)[11,12] and (M = Ag, Au, and $n$ = 1, 3, 5),[12] show that the excitation spectra of CuCN, AgCN, and

**Received:** July 19, 2012
**Published:** September 6, 2012

   dx.doi.org/10.1021/ja307087d | J. Am. Chem. Soc. 2012, 134, 16387−16400

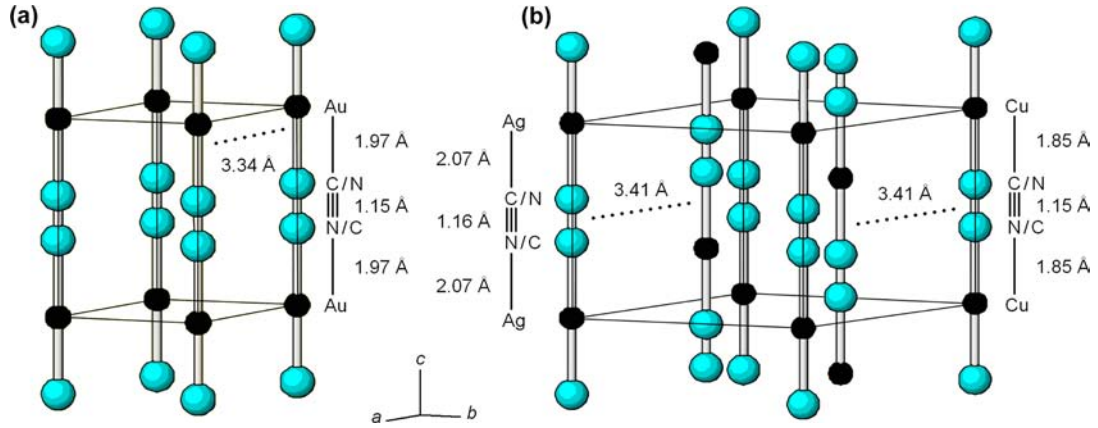


**Figure 1.** Structures of (a) gold cyanide (AuCN) in space group *P6/mmm* and (b) high-temperature copper cyanide (HT-CuCN) and silver cyanide (AgCN) in space group $R\bar{3}m$. Key: copper, silver, and gold, black spheres; head-to-tail disordered cyanide, cyan spheres. The C≡N, M−C/N, and interchain distances are shown for all compounds at 10 K.[1,4,5]

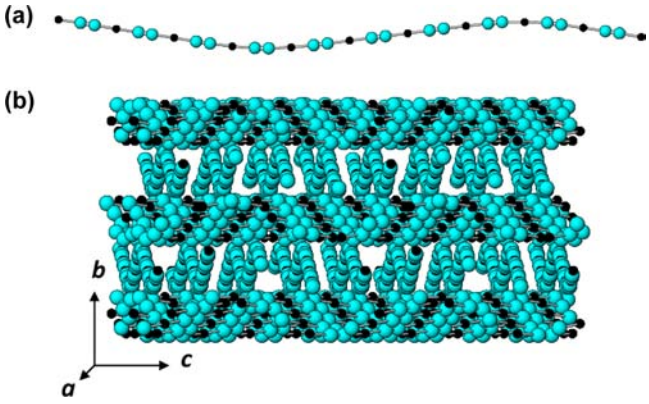


**Figure 2.** Structure of low-temperature copper cyanide (LT-CuCN) showing (a) a single wave-like $[Cu-C\equiv N-]_n$ chain and (b) the packing of the chains into layers.[3] Key as for Figure 1.

AuCN can in part be attributed to Laporte-allowed $\pi-\pi^*$ transitions. We note that these calculations neglect any interactions between the chains. These interchain interactions are likely to be highly significant, as shown by the work of Rawashdeh-Omary et al. concerning the spectra of the $[Ag(CN)_2]^-$ and $[Au(CN)_2]^-$ ions, which show red shifts of $\sim 10^4$ $cm^{-1}$ in the lowest-energy absorption bands on increasing their concentrations from $\sim 10^{-3}$ to 1 M.[13,14] The large changes in the absorption spectra are ascribed to association of the $[Ag(CN)_2]^-$ and $[Au(CN)_2]^-$ ions caused by argento- and aurophilic interactions. Other photophysical measurements of relevance to this work have been made on the mixed silver−gold compounds, $La[Ag_xAu_{1-x}(CN)_2]_3 \cdot 3H_2O$, containing $[Ag(CN)_2]^-$ and $[Au(CN)_2]^-$ units, in which the luminescence properties can be tuned by varying $x$.[15−17]

This paper describes the preparation and characterization of phases of the form $(M_xM'_{1-x})CN$ (M, M′ = Cu, Ag, Au), which contain mixed-metal−cyanide chains packed in structures closely related to those of the parent cyanides, HT-CuCN, AgCN, and AuCN. The phase limits for the mixed-metal systems have been established and their thermal expansion properties measured. All the compounds, like their parents, show 1-D NTE, the magnitude of which can be related to the composition and packing of the mixed-metal chains. The IR and Raman spectra of $(Ag_{1/2}Au_{1/2})CN$ have been measured previously,[18,19] but the conclusions drawn regarding the symmetry of the chains were incorrect (*vide infra*), and no structural information was reported. In the present paper, the vibrational spectra of all the mixed-metal cyanides are analyzed and provide information on the metal and cyanide ordering occurring within the chains.

In certain gold-containing compounds, $(Cu_{1/2}Au_{1/2})CN$ and $(Cu_{2/3}Au_{1/3})CN$, we find that there is complete ordering of the metal atoms and cyanide groups within individual chains. However, the lack of long-range order between chains in these systems means that detailed structural information, including whether C or N is preferentially bonded to gold and the M−C and M′−N distances, cannot be obtained from simple Bragg diffraction studies. We therefore use total neutron diffraction to study $(Cu_{1/2}Au_{1/2})CN$ and $(Ag_{1/2}Au_{1/2})CN$, in addition to $(Cu_{0.50}Ag_{0.50})CN$, to determine both their local and long-range structures. The results, in combination with those of the diffuse reflectance spectroscopy, show that aurophilic interactions do not appear to be necessary to cause the gold-containing materials $(Ag_{1/2}Au_{1/2})CN$ and $(Cu_{1/2}Au_{1/2})CN$ to adopt the AuCN structure type.

The diffuse reflectance spectra and photoluminescent behaviors of the mixed-metal and parent cyanides have also been investigated. It is notable that the diffuse reflectance spectra of LT-CuCN, AgCN, and AuCN have not been previously reported, which is surprising given the different colors of these compounds and the importance of absorption spectra for photoluminescent studies. Luminescent lifetimes are measured for the first time for LT-CuCN and AuCN, as well the mixed-metal cyanides. We conclude that the photophysical properties of both the new mixed-metal cyanides and their parents are influenced by both intra- and interchain ordering. In particular, interchain interactions must be responsible for the yellow color of AuCN.

## ■ RESULTS AND DISCUSSION

The structure types and lattice parameters of the single-phase polycrystalline materials, $(M_xM'_{1-x})CN$, prepared at room temperature from aqueous cyanide solutions, were determined using powder X-ray diffraction (PXRD) (Tables 1 and S.3), and the compositions of the $(Cu_xAg_{1-x})CN$ compounds were confirmed using atomic absorption spectroscopy (Table S.2). In the CuCN−AgCN system, a solid solution, $(Cu_xAg_{1-x})CN$, exists over the range $0 \le x \le 1$, whereas in the AgCN−AuCN system, only a single intermediate, a line phase with


dx.doi.org/10.1021/ja307087d | J. Am. Chem. Soc. 2012, 134, 16387−16400

**Table 1. Mixed-Metal Cyanide Compounds, $(M_xM'_{1-x})CN$ (M, M′ = Cu, Ag, Au), Their Structure Types, and Hexagonal Lattice Parameters Determined at Room Temperature**

| composition[a] | color | structure type | $a$/Å | $c$/Å |
|---|---|---|---|---|
| HT-CuCN[b] | off-white | AgCN | 6.031(2) | 4.829(3) |
| AgCN | white | AgCN | 6.007(2) | 5.259(3) |
| AuCN | bright yellow | AuCN | 3.393(9) | 5.066(7) |
| $(Cu_{0.17}Ag_{0.83})CN$ | white | AgCN | 6.022(3) | 5.201(5) |
| $(Cu_{0.33}Ag_{0.67})CN$ | white | AgCN | 6.031(2) | 5.108(3) |
| $(Cu_{0.50}Ag_{0.50})CN$ | white | AgCN | 6.022(5) | 5.007(5) |
| $(Cu_{0.67}Ag_{0.33})CN$ | white | AgCN | 6.030(9) | 4.926(11) |
| $(Cu_{0.83}Ag_{0.17})CN$ | white | AgCN | 6.026(3) | 4.877(3) |
| $(Cu_{0.93}Ag_{0.07})CN$[b] | off-white | AgCN | 6.031(3) | 4.845(3) |
| $(Cu_{1/2}Au_{1/2})CN$ | pale yellow | AuCN | 3.396(5) | 4.931(6) |
| $(Cu_{7/12}Au_{5/12})CN$ | pale yellow | AuCN | 3.421(3) | 4.918(4) |
| $(Cu_{2/3}Au_{1/3})CN$ | pale yellow | AuCN | 3.424(5) | 4.882(5) |
| $(Ag_{1/2}Au_{1/2})CN$ | white | AuCN | 3.425(5) | 5.158(6) |

[a]Compositions of line phases are indicated by the use of fractions in the formulas. Members of solid solutions have their compositions expressed as decimals. [b]High-temperature polymorph with AgCN structure formed on heating as-synthesized material at 320 °C under vacuum for 2 h.

composition $(Ag_{1/2}Au_{1/2})CN$, is formed. In the Cu−Au system, there are line phases at $(Cu_{2/3}Au_{1/3})CN$ and $(Cu_{1/2}Au_{1/2})CN$. Between these phases, it appears that additional phases, such as $(Cu_{7/12}Au_{5/12})CN$, may exist as line phases.

**Powder X-ray Diffraction.** *CuCN−AgCN Phases.* The PXRD patterns of compounds in the CuCN−AgCN system (Table 1 and Figure 3), prepared both at room temperature (0

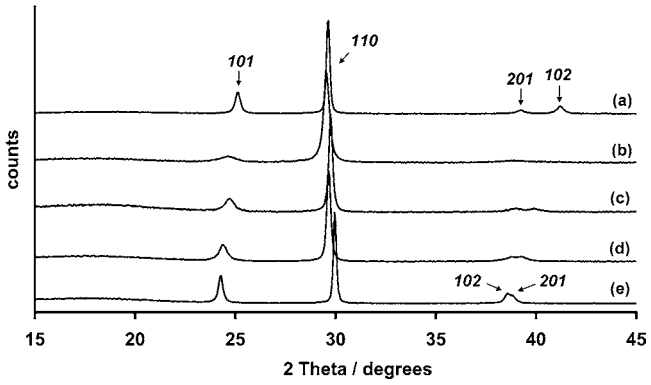


**Figure 3.** Indexed PXRD patterns measured at room temperature of (a) HT-CuCN, (b) $(Cu_{0.67}Ag_{0.33})CN$, (c) $(Cu_{0.50}Ag_{0.50})CN$, (d) $(Cu_{0.33}Ag_{0.67})CN$, and (e) AgCN.

$\leq x \leq 0.83$) and after heating the low-temperature phases ($0.93 \leq x \leq 1$), can be indexed on the basis of simple hexagonal lattice parameters with $a = b \approx 6$ Å and $c \approx 5$ Å. This indicates that they all have the AgCN (HT-CuCN) structure (Figure 1b). There is a steady decrease in the $c$ lattice parameter as a function of increasing copper content, with no evidence for discontinuities (Figure 4). This behavior confirms that the $(Cu_xAg_{1-x})CN$ system forms a solid solution. There is a slight negative deviation from ideal Vegard's law behavior (dashed line), suggesting true miscibility of CuCN and AgCN at room temperature and the occurrence of enhanced interactions within the mixed-metal chains on formation of the solid

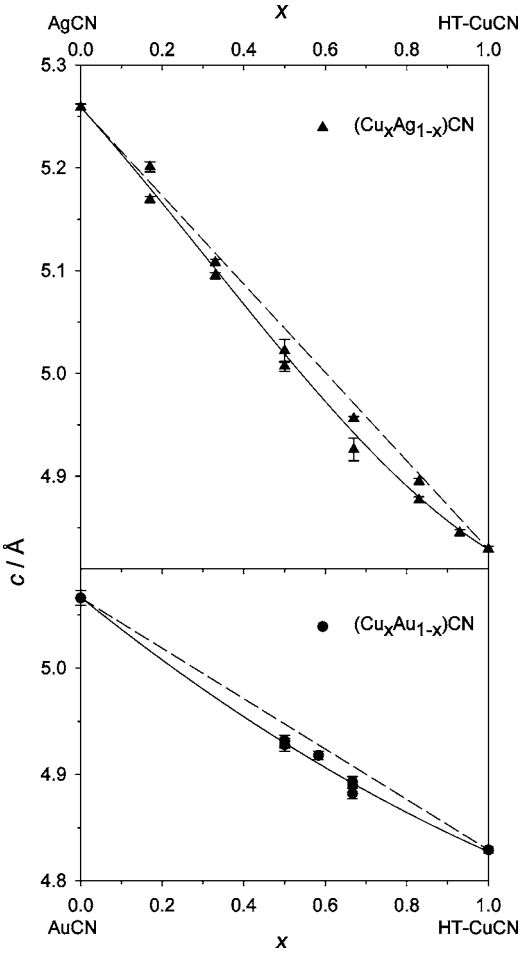


**Figure 4.** Variation with $x$ of the $c$ lattice parameters of $(Cu_xAg_{1-x})CN$ (▲) and $(Cu_xAu_{1-x})CN$ (●). The continuous line is a cubic fit to the data, and the dashed line is a straight line between the end points.

solution.[20] A likely explanation is that, in the mixed-metal chains, the C≡N groups can order locally into Cu−N≡C−Ag or Cu−C≡N−Ag linkages. This behavior is in contrast with that of the single-metal parents, CuCN[7] and AgCN,[8] in which the C≡N groups are found to be head-to-tail disordered.

At very high copper concentrations ($0.93 \leq x \leq 1$), the compounds initially formed by the acid addition procedure have the LT-CuCN structure (Figure 2). These convert to the AgCN (HT-CuCN) structure on heating to 320 °C under vacuum, establishing that the solid solution exists over the full composition range ($0 \leq x \leq 1$). In HT-CuCN and AgCN, the $c$ lattice parameters correspond to the bond length sum of $2r_{M-C/N} + r_{C\equiv N}$ (Figure 1). The decrease in the $c$ parameter with increasing $x$ in the mixed CuCN−AgCN series thus reflects the fact that Cu−C/N bonds ($r_{Cu-C/N} = 1.85$ Å) are shorter than Ag−C/N bonds ($r_{Ag-C/N} = 2.07$ Å).[1,4] The lattice parameter $a$ (Table 1), and the corresponding derived interchain distance $a/\sqrt{3}$ (Figure S.1), vary little with composition, as might be expected given the similarity of the $a$ lattice parameters of HT-CuCN and AgCN.

*AgCN−AuCN Phases.* In the exploration of the AgCN−AuCN system using acid precipitation (Table S.5, Figure S.2), only a single mixed-metal compound was formed, namely, a line phase with composition $(Ag_{1/2}Au_{1/2})CN$ (Table 1). Attempts to make gold-rich compositions resulted in the formation of the $(Ag_{1/2}Au_{1/2})CN$ solid phase and $HAu(CN)_2$


dx.doi.org/10.1021/ja307087d | J. Am. Chem. Soc. 2012, 134, 16387−16400

in solution. The latter decomposed after several days to precipitate AuCN. In contrast, at the silver-rich end of the composition range, AgCN is formed in addition to $(Ag_{1/2}Au_{1/2})CN$. $(Ag_{1/2}Au_{1/2})CN$ can also be made in a rational manner by the stoichiometric reaction between $[Au(CN)_2]^-$ and $Ag^+$ ions. The PXRD pattern of this phase can be indexed on a hexagonal unit cell similar to that of AuCN, showing that $(Ag_{1/2}Au_{1/2})CN$ adopts the AuCN structure rather than that of AgCN (Figure 5). The *c* lattice

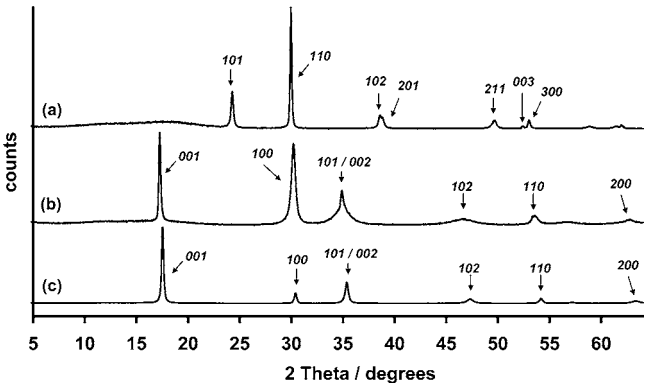


**Figure 5.** Indexed PXRD patterns measured at room temperature of (a) AgCN, (b) $(Ag_{1/2}Au_{1/2})CN$, and (c) AuCN.

parameter for $(Ag_{1/2}Au_{1/2})CN$ is close to the average of the values for the parent cyanides, AgCN and AuCN. The interchain distance in $(Ag_{1/2}Au_{1/2})CN$, which corresponds to the *a* lattice parameter, is just below the mean of the interchain distances in the parent compounds (Table S.5).

Although the formation of a single mixed-metal phase of 1:1 stoichiometry suggests that the chains in $(Ag_{1/2}Au_{1/2})CN$ are ordered, there is no evidence from the Bragg diffraction data that this is the case; i.e., no additional superlattice reflections occur in the powder pattern, and consequently the unit cell still contains only one MCN unit. It should be noted that the absence of superlattice reflections does not preclude ordering within individual chains if there is no long-range interchain order.

*CuCN–AuCN Phases.* A line phase with 1:1 ratio of the parents, $(Cu_{1/2}Au_{1/2})CN$, was formed in the CuCN–AuCN system. No further solid phases were found toward the AuCN-rich end of the phase diagram, but, as was found in the acid precipitation experiments in the AgCN–AuCN system, the excess gold present formed $HAu(CN)_2$. However, in the CuCN-rich region of the phase diagram, with $x \geq 2/3$, a second line phase, $(Cu_{2/3}Au_{1/3})CN$, was prepared in combination with LT-CuCN. Both line phases have the AuCN structure type, as seen from their PXRD patterns, which can be indexed on the basis of simple hexagonal lattice parameters with $a = b \approx 3.4$ Å and $c \approx 5$ Å (Table 1, Figure 6). The *c* lattice parameters for these two line phases are both a little shorter (~0.02 Å) than the weighted averages of the *c* lattice parameters of the parents (Figure 4). A material was prepared at a composition between those of the two line phases, $(Cu_{1/2}Au_{1/2})CN$ and $(Cu_{2/3}Au_{1/3})CN$, with a CuCN:AuCN ratio of 7/12:5/12. The indexed powder pattern yielded a *c* parameter intermediate between those of $(Cu_{1/2}Au_{1/2})CN$ and $(Cu_{2/3}Au_{1/3})CN$, showing that at least one additional line phase or a range of solid solution must exist in this region.

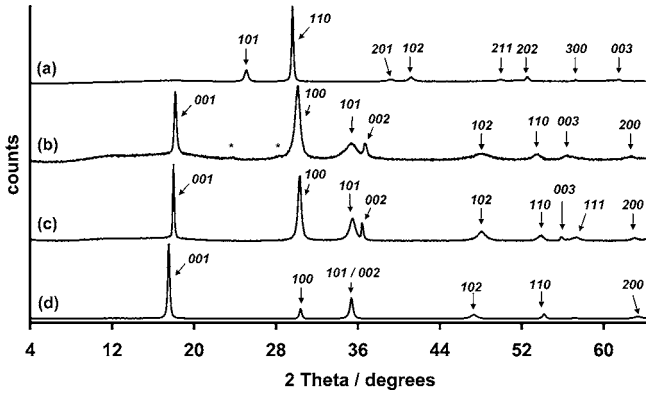


**Figure 6.** Indexed PXRD patterns measured at room temperature of (a) HT-CuCN, (b) $(Cu_{2/3}Au_{1/3})CN$, (c) $(Cu_{1/2}Au_{1/2})CN$, and (d) AuCN, showing that the mixed-metal phases all have the AuCN structure type. * indicates small amount of LT-CuCN present as impurity.

Again the absence of superlattice reflections in the PXRD patterns for the mixed copper–gold phases shows that these materials lack long-range interchain order, but in this system, the existence of line phases is highly suggestive of order in individual chains. The full structural characterization of $(Cu_{1/2}Au_{1/2})CN$ requires total neutron diffraction studies and is presented below, together with those of $(Ag_{1/2}Au_{1/2})CN$ and $(Cu_{0.50}Ag_{0.50})CN$.

**Vibrational Spectroscopy.** Vibrational spectroscopy can, in contrast to PXRD, yield information on the order and connectivity *within* metal–cyanide chains, even if there is no long-range order *between* the chains.

The parent cyanides, HT-CuCN, AgCN, and AuCN, all give rise to a principal $\nu_{C\equiv N}$ vibration observable in both the infrared and Raman spectra (Table 2). It is notable that they

**Table 2. Principal Stretching Frequencies, $\nu_{C\equiv N}$, Observed in Infrared and Raman Spectra for the Single-Metal and Mixed-Metal Cyanides[a]**

| | $\nu_{C\equiv N}/cm^{-1}$ | |
|---|---|---|
| composition | IR | Raman |
| LT-CuCN | 2166 | 2177 [3] |
| HT-CuCN | 2168 | 2172 |
| AgCN | 2161 | 2167 |
| AuCN | 2234 | 2236 |
| $(Cu_{0.17}Ag_{0.83})CN$ | 2167 | 2173 |
| $(Cu_{0.33}Ag_{0.67})CN$ | 2167 | 2173 |
| $(Cu_{0.50}Ag_{0.50})CN$ | 2167 | 2173 |
| $(Cu_{0.67}Ag_{0.33})CN$ | 2166 | 2172 |
| $(Cu_{0.83}Ag_{0.17})CN$ | 2165 | 2169 |
| $(Cu_{2/3}Au_{1/3})CN$ | 2208, 2190(sh), 2167 | 2226, 2193, 2171 |
| $(Cu_{7/12}Au_{5/12})CN$ | 2207, 2189(sh), 2165(sh) | 2226, 2193, 2173 |
| $(Cu_{1/2}Au_{1/2})CN$ | 2208 | 2226 |
| $(Ag_{1/2}Au_{1/2})CN$ | 2208 | 2225 |

[a]sh = shoulder.

are coincident for each compound. Bowmaker[21] used the coincidence of the $\nu_{C\equiv N}$ stretch in the IR and Raman spectra of CuCN, AgCN, and AuCN as evidence for ordered chains of the form $[M-CN-M-CN-]_n$, but this coincidence is also consistent with the existence of head-to-tail disorder of the C≡N groups in the chains, as has been shown to exist by


dx.doi.org/10.1021/ja307087d | J. Am. Chem. Soc. 2012, 134, 16387–16400

NMR experiments on CuCN[7] and AgCN.[8] In HT-CuCN and AgCN, the $\nu_{C\equiv N}$ stretching frequencies in the IR and Raman spectra are similar but occur at a wavenumber ~70 $cm^{-1}$ lower than those found for AuCN, in agreement with values reported previously.[18,19,21,22] On formation of the mixed Cu−Au and Ag−Au cyanide phases, significant changes occur in the $\nu_{C\equiv N}$ stretching frequencies observed in the IR and Raman spectra, yielding information on both metal and cyanide ordering within the metal−cyanide chains. In contrast, there is negligible change in the $\nu_{C\equiv N}$ vibrational frequency on the formation of the mixed $(Cu_xAg_{1-x})CN$ compounds. However, information on order within the metal−cyanide chains in these compounds can be obtained by examination of the changes in the $\nu_{M-C/N}$ stretching frequencies observed at lower wavenumbers in the Raman spectra.

*$(Cu_{1/2}Au_{1/2})CN$ and $(Ag_{1/2}Au_{1/2})CN$.* The values for the stretching frequencies, $\nu_{C\equiv N}$, obtained from the IR and Raman spectra are noncoincident in either $(Cu_{1/2}Au_{1/2})CN$ (Table 2, Figure S.4) or $(Ag_{1/2}Au_{1/2})CN$ (Table 2, Figure 7), showing

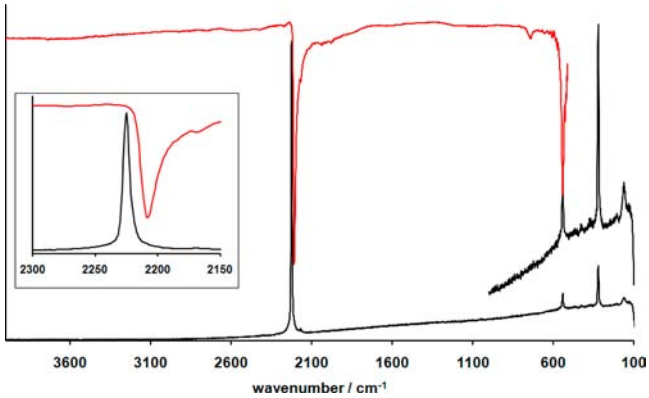


**Figure 7.** IR (red) and Raman (black) spectra of $(Ag_{1/2}Au_{1/2})CN$, with inset showing the noncoincidence of the $\nu_{C\equiv N}$ stretching vibrations.

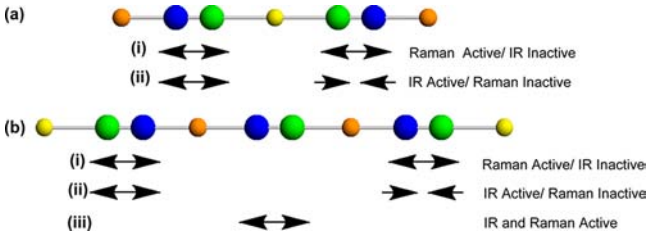


**Figure 8.** IR- and Raman-active $\nu_{C\equiv N}$ stretching vibrational modes in (a) ordered $(M_{1/2}M'_{1/2})CN$, $D_{\infty h}$ chains, and (b) ordered $(M_{2/3}M'_{1/3})CN$, $C_{\infty v}$ chains. Key: metal M, orange; metal M′, yellow; carbon, green; and nitrogen, blue.

that the individual chains in each compound are centrosymmetric (Figure 8a). Frankiss et al. had previously failed to identify the center of symmetry in $(Ag_{1/2}Au_{1/2})CN$.[18,19] The existence of the center of symmetry, together with the fact that only one $\nu_{C\equiv N}$ frequency is observed in each spectrum, shows that there must be strict alternation of the metal atoms within the chains, i.e., (M···M′···M···M′), together with cyanide ordering. The existence of a single C≡N environment in each of the compounds is further confirmed by the observation of only one $\nu_{M-C/N}$ stretching frequency, which occurs at 606 $cm^{-1}$ (IR) and 593 $cm^{-1}$ (R) for $(Cu_{1/2}Au_{1/2})CN$, and at 540 $cm^{-1}$ in both spectra for $(Ag_{1/2}Au_{1/2})CN$. These $\nu_{M-C/N}$ values, as might be expected, lie intermediate between those for the parent compounds, which occur at 591 $cm^{-1}$ for CuCN, 480 $cm^{-1}$ for AgCN, and 598 $cm^{-1}$ for AuCN.[21] The bending vibrations at 337 and 254 $cm^{-1}$ in the Raman spectrum of $(Cu_{1/2}Au_{1/2})CN$ and at 321 and 160 $cm^{-1}$ in that of $(Ag_{1/2}Au_{1/2})CN$ are assigned to $\delta_{MCN}$ and $\delta_{NMC}$, and are also shifted compared to those of the parents.[21]

Unfortunately, vibrational spectroscopy does not yield the sense of the cyanide binding, which may be either M′−N≡C−M−C≡N−M′ or M′−C≡N−M−N≡C−M′. To determine whether the chains in $(Ag_{1/2}Au_{1/2})CN$ are of the form $[Ag-CN-Au-NC-]_n$ or $[Ag-NC-Au-CN-]_n$, and whether those in $(Cu_{1/2}Au_{1/2})CN$ are $[Cu-CN-Au-NC-]_n$ or $[Cu-NC-Au-CN-]_n$, additional experiments are required. In the following section, the results of total neutron diffraction are used to determine the sense of the cyanide binding and the metal−carbon and metal−nitrogen bond lengths in these disordered materials.

*$(Cu_{2/3}Au_{1/3})CN$ and $(Cu_{7/12}Au_{5/12})CN$.* The assumption is made in the following discussion that, in the Cu−Au cyanide systems, the carbon end of the cyanide group is attached to gold. This is proved to be correct in the case of $(Cu_{1/2}Au_{1/2})$-CN by using total diffraction techniques, as described below. The IR and Raman spectra of $(Cu_{2/3}Au_{1/3})CN$ and $(Cu_{7/12}Au_{5/12})CN$ (Table 2, Figure S.5) can be interpreted by comparison with the spectra obtained for $(Cu_{1/2}Au_{1/2})CN$ and the simple metal cyanides, CuCN and AuCN. The $\nu_{C\equiv N}$ stretching frequencies at 2208 $cm^{-1}$ (IR) and 2226 $cm^{-1}$ (R) for $(Cu_{2/3}Au_{1/3})CN$, and at 2207 $cm^{-1}$ (IR) and 2226 $cm^{-1}$ (R) for $(Cu_{7/12}Au_{5/12})CN$, are assigned as the asymmetric and symmetric vibrations of the cyanide groups bridging between gold and copper in Cu−NC−Au−CN−Cu units, as shown in Figure 8a. The vibration at 2190 $cm^{-1}$ (IR), coincident with 2193 $cm^{-1}$ (R) and observed for both $(Cu_{2/3}Au_{1/3})CN$ and $(Cu_{7/12}Au_{5/12})CN$, is assigned to the stretching of the C≡N group bonded between copper atoms in Au−CN−Cu−C≡N−Cu−NC−Au units (Figure 8b-iii). The final stretching vibration seen in the region 2165−2171 $cm^{-1}$ in the IR and Raman spectra of both compounds can only be accounted for by considering the occurrence of longer sequences of $(Cu-C\equiv N-)_n$ units within the chains (Figure 9). In both HT- and LT-CuCN, the analogous $\nu_{C\equiv N}$ stretch also occurs at ~2167 $cm^{-1}$. It should be noted that the absence of a $\nu_{C\equiv N}$ stretching vibration at ~2235 $cm^{-1}$ in the IR and/or Raman spectra

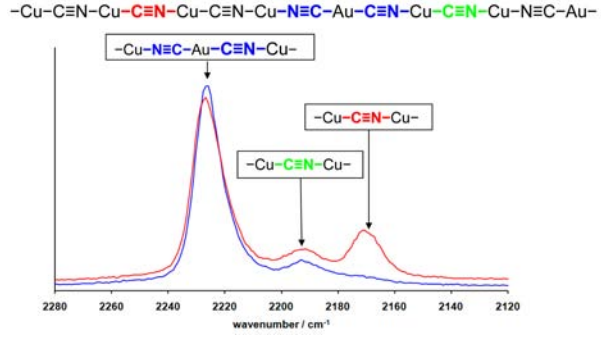


**Figure 9.** Raman spectra of $(Cu_{2/3}Au_{1/3})CN$ (red) and $(Cu_{7/12}Au_{5/12})$-CN (blue) over the range 2120−2280 $cm^{-1}$, together with a possible metal sequence within the copper−gold chains which accounts for the observed $\nu_{C\equiv N}$ stretching vibrations.


dx.doi.org/10.1021/ja307087d | J. Am. Chem. Soc. 2012, 134, 16387−16400

suggests that Au−CN−Au linkages are never formed in $(Cu_{2/3}Au_{1/3})CN$ and $(Cu_{7/12}Au_{5/12})CN$.

*$(Cu_xAg_{1-x})CN$.* In the solid solution, $(Cu_xAg_{1-x})CN$, the $\nu_{C\equiv N}$ stretch is coincident in the Raman and IR spectra at ~2170 $cm^{-1}$ (Table 2, Figures S.6 and S.7), with no significant variation in frequency with $x$. This value is close to those seen for the parent cyanides, CuCN and AgCN. Thus, even at the composition $(Cu_{0.50}Ag_{0.50})CN$, there must be metal and cyanide disorder within the metal−cyanide chains, in contrast to the behavior in $(Cu_{1/2}Au_{1/2})CN$ and $(Ag_{1/2}Au_{1/2})CN$ described above.

In the $(Cu_xAg_{1-x})CN$ system, both the $\nu_{M-C/N}$ stretches, seen in the Raman spectra in the range 450−600 $cm^{-1}$ (Figure 10), and the bending motions, for example, $\delta_{MCN}$ and $\delta_{NMC}$,

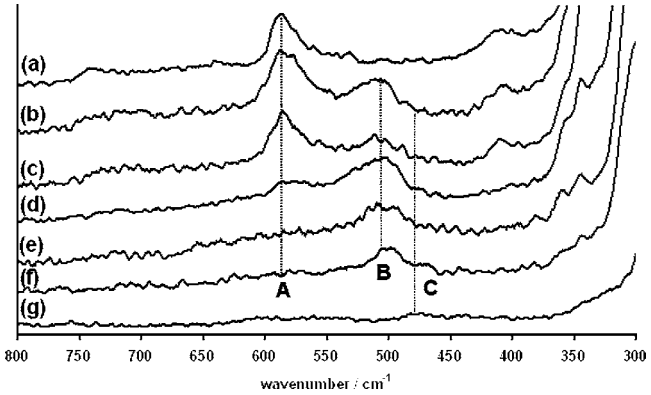


**Figure 10.** Raman data for mixed copper−silver cyanides and parent compounds: (a) LT-CuCN, (b) $(Cu_{0.87}Ag_{0.13})CN$, (c) $(Cu_{0.67}Ag_{0.33})CN$, (d) $(Cu_{0.50}Ag_{0.50})CN$, (e) $(Cu_{0.33}Ag_{0.67})CN$, (f) $(Cu_{0.13}Ag_{0.87})CN$, and (g) AgCN. Vertical dashed lines: band A, the Cu−C/N stretch in the Cu−CN−Cu unit;[21] band B, the Cu−N stretch (which is also the Ag−C stretch) in the Cu−NC−Ag unit (assigned on the basis of arguments given in the neutron diffraction section below); and band C, the Ag−C/N stretch in the Ag−CN−Ag unit.[21]

seen below 400 $cm^{-1}$ (Figure S.8), are at substantially different wavenumbers from those of the parent compounds. Analysis of the $\nu_{M-C/N}$ stretches is straightforward and provides information on the local structure within the chains. In the parent cyanides, the $\nu_{M-C/N}$ stretches are at 590 $cm^{-1}$ (CuCN) (Figure 10, band A) and 480 $cm^{-1}$ (AgCN)[21] (Figure 10, band C). In all the mixed Cu−Ag cyanides, an intermediate band appears at ~510 $cm^{-1}$ (Figure 10, band B), which can be assigned as arising from a $\nu_{M-C/N}$ stretch from either Cu−NC−Ag or Cu−CN−Ag linkages. Chemical intuition suggests that C≡N order is likely to occur in the sense Cu−N≡C−Ag. This is indeed shown to be correct from our total neutron diffraction studies.

It is notable that band A does not appear in the Raman spectra of either $(Cu_{0.33}Ag_{0.67})CN$ or $(Cu_{0.13}Ag_{0.87})CN$ (Figure 10e,f), showing that the Cu−CN−Cu linkage does not occur at low copper concentration and that there is a preference for Cu to have Ag atoms as nearest metal neighbors within the chains. At the composition $(Cu_{0.50}Ag_{0.50})CN$, the appearance of band A (Figure 10d) shows that there must be a small number of Cu−CN−Cu linkages in addition to the Cu−NC−Ag linkages seen at band B. Thus, there is more than one type of link present in the chain, and perfect alternation of metals along the chains, i.e., Cu−NC−Ag−CN−Cu−NC−Ag−, does not occur. The band expected to be observed at C in Figure 10d, corresponding to the $\nu_{Ag-C/N}$ stretch in the Ag−CN−Ag unit in these materials, is only of very low intensity in the parent AgCN (Figure 10g) and, hence, is not seen in the mixed-metal phases. The occurrence of more than one cyanide environment in $(Cu_{0.50}Ag_{0.50})CN$ contrasts with the cases of $(Cu_{1/2}Au_{1/2})CN$ and $(Ag_{1/2}Au_{1/2})CN$, where there is complete order.

**Total Neutron Diffraction Studies of $(Cu_{1/2}Au_{1/2})CN$, $(Ag_{1/2}Au_{1/2})CN$, and $(Cu_{0.50}Ag_{0.50})CN$.** As we have shown above, the information obtainable from Bragg diffraction for the mixed-metal cyanides, all of which are disordered crystalline materials, is rather limited and has to be supplemented by other methods. For example, we have used vibrational spectroscopy to demonstrate the existence of complete metal and cyanide ordering within individual $[M-CN-M'-NC]_n$ chains in the gold-containing systems $(Cu_{1/2}Au_{1/2})CN$ and $(Ag_{1/2}Au_{1/2})CN$, and incomplete metal and cyanide ordering within the chains in $(Cu_{0.50}Ag_{0.50})CN$. To explore structure−property relationships in these materials, their local structures need to be determined. This can be done using total diffraction techniques, using either X-rays or neutrons, which yield directly model-independent information on pair correlation functions. This information is particularly useful to the chemist, as at short distances, peaks in the correlation function can be assigned to distinct pairs of atoms and hence produce bond distances directly.[23,24]

Because the atomic numbers (and hence X-ray scattering powers) of C and N are very similar, and significantly lower than those of the metals, particularly Au, total neutron diffraction is needed to determine the preferred arrangement for CN binding within the mixed-metal chains, e.g., as either Cu−C≡N−Au or Cu−N≡C−Au. (The coherent neutron scattering lengths, $\bar{b}$, for Cu, Ag, Au, C, and N are 7.718, 5.922, 7.63, 6.6460, and 9.36 fm, respectively.[25]) A further important issue to be addressed is whether the adoption by $(Cu_{1/2}Au_{1/2})CN$ and $(Ag_{1/2}Au_{1/2})CN$ of the AuCN structure, in which the metal atoms lie in sheets (Figure 1), is controlled by aurophilic interactions. Although the lack of superlattice reflections in the Bragg diffraction patterns of $(Cu_{1/2}Au_{1/2})CN$ and $(Ag_{1/2}Au_{1/2})CN$ precludes long-range order between the chains, which if present would generate alternating homometallic sheets in these systems, it is still possible that there is a local preference in neighboring chains for Au···Au interactions (with necessarily occurring Cu···Cu and Ag···Ag interactions), rather than Au···Ag and Au···Cu interactions. Total diffraction has the potential to determine whether such local metal ordering occurs.

**Intrachain Order.** Figure 11 shows the low-$r$ region of the neutron correlation functions, $T^N(r)$, for the three mixed-metal compounds, obtained using a value of 50 $Å^{-1}$ for $Q_{max}$. In each of these functions, the first peak at ~1.15 Å can be unambiguously assigned to the C≡N distance in cyanide groups. The peak manifold in the region ~1.7−2.2 Å corresponds to short correlations from carbon and nitrogen directly bonded to a metal. For $(Cu_{1/2}Au_{1/2})CN$ and $(Cu_{0.50}Ag_{0.50})CN$, there are clearly two peaks in this region, while for $(Ag_{1/2}Au_{1/2})CN$, the two peak components are too close to be resolved.

For $(Cu_{1/2}Au_{1/2})CN$ and $(Cu_{0.50}Ag_{0.50})CN$, the metals involved in the correlations giving rise to each of the two peaks can be unambiguously assigned by reference to the bond lengths previously observed in the parent compounds (Table 3). Thus, the peaks at lower $r$ (~1.8 Å) arise from Cu−C/N correlations, and those at higher $r$ (~2 Å) from Ag−C/N and Au−C/N correlations.


dx.doi.org/10.1021/ja307087d | J. Am. Chem. Soc. 2012, 134, 16387−16400

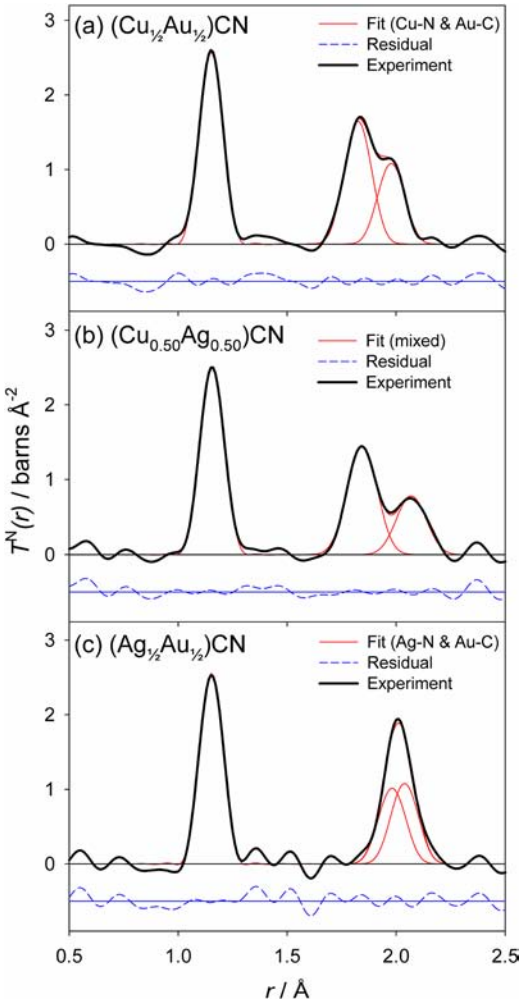


**Figure 11.** Final fits to the low-$r$ region of the total neutron correlation function, $T^N(r)$, for (a) $(Cu_{1/2}Au_{1/2})CN$, (b) $(Cu_{0.50}Ag_{0.50})CN$, and (c) $(Ag_{1/2}Au_{1/2})CN$ at 10 K. The experimental data are shown by a thick continuous black line, while the best fit (components and total) is shown by a thin continuous red line, and the fit residual is shown by a shifted dashed blue line.

Because C and N have significantly different neutron scattering lengths, it is possible, in the cases of $(Cu_{1/2}Au_{1/2})CN$ and $(Cu_{0.50}Ag_{0.50})CN$, to determine the sense of the cyanide binding by fitting the two components of the M−C/N manifold. The simplest aspect to consider is that the area of each component of the manifold depends on the atom pairs involved as $(\overline{b}_M \times \overline{b}_C)$ and $(\overline{b}_{M'} \times \overline{b}_N)$. Another important point to note is that the fitted widths of both components (a measure of the root-mean-square deviation of the bond length) must be physically reasonable and also approximately equal. Thus, for $(Cu_{1/2}Au_{1/2})CN$, the best fit to the low-$r$ region of $T^N(r)$ is obtained when Cu is bonded to N and Au to C (Figure 11a, Table 3). A favorable feature of the fit is that the two peak widths, $u_{Cu-N}$ and $u_{Au-C}$, are equal within one standard deviation and are very similar to those measured previously for the parent compounds, HT-CuCN and AuCN (Table 3). The associated coordination numbers, $n_{Cu-N}$ and $n_{Au-C}$, which were constrained to be equal during the fit, are only slightly smaller than the expected value of 2. (Experimental coordination numbers are usually slightly smaller than the ideal values for reasons explained previously.[28]) Reversing the orientation of the cyanide group (i.e., assuming Cu−C and Au−N bonds; Figure S.11, Table S.7) gives an inferior fit in which the two peak widths are not only very different, but in one case unfeasibly large, and inconsistent with the values observed in the parent compounds.

The low-$r$ region of $T^N(r)$ for $(Cu_{0.50}Ag_{0.50})CN$ was fitted according to the two fully ordered models (Cu−NC−Ag−CN−Cu and Cu−CN−Ag−NC−Cu), with the coordination numbers of the two metals again constrained to be equal. The fit for the model containing Cu−C and Ag−N bonds may be rejected because the peak widths $u_{Cu-C}$ and $u_{Ag-N}$ (Figure S.11c, Table S.7), when considered together, are unreasonable. The fit for the model with Cu−N and Ag−C bonds is much improved because the peak widths $u_{Cu-N}$ and $u_{Ag-C}$ are similar (Figure S.11b, Table 3) and are of reasonable magnitude.

However, it was shown above from the Raman data that the chains in $(Cu_{0.50}Ag_{0.50})CN$ cannot be fully ordered. The introduction of a small number of Cu−C and Ag−N bonds (the "mixed model") improved the fit still further. Figure 11b shows the low-$r$ region of $T^N(r)$ for $(Cu_{0.50}Ag_{0.50})CN$ fitted using the mixed model (Table 3), with the two peak widths constrained to be equal. The best fit is obtained when 85% of atoms bonded to Cu are N and 15% are C.

Although the difference between the M−C/N bond lengths in AgCN and AuCN is only 0.096 Å (Table 3), this difference, if maintained in $(Ag_{1/2}Au_{1/2})CN$, would be sufficient to allow the sense of the C≡N binding to be determined using the approach described above. However, in $(Ag_{1/2}Au_{1/2})CN$, inspection of $T^N(r)$ shows that the difference in the M−C and M′−N bond lengths is significantly reduced so that the peak at ∼2 Å in $T^N(r)$ cannot be separated into two contributions (Figure 11c). The low-$r$ region of $T^N(r)$ for $(Ag_{1/2}Au_{1/2})CN$ was therefore fitted using the two possible ordered models (Ag−NC−Au−CN−Ag and Ag−CN−Au−NC−Ag), with the coordination numbers of the two metals, $n_{j-k}$, and the corresponding peak width values, $u_{j-k}$, constrained to be equal. The two models produce fits with very similar $R$ factors (Table S.7). The preferred final model (Figure 11c, Table 3) was chosen because the ratio $n_{Au-C}:n_{C\equiv N}$ is closer to 2 than $n_{Au-N}:n_{C\equiv N}$ and, more compellingly, because Meng et al.[29] found from $^{13}C$ NMR that a short silver−gold−cyanide anion chain fragment, when encapsulated into the tubular cavity of a copper(I)−amine host, ordered as $(NC-Au-CN-Ag-NC-Au-CN)^-$. The corresponding encapsulated copper−gold chain fragment was found to order as $(NC-Au-CN-Cu-NC-Au-CN)^-$, with cyanide bound in the same sense as determined in our extended chain system, $(Cu_{1/2}Au_{1/2})CN$.

**Interchain Order in the Gold-Containing Compounds.** The question of interchain order is particularly meaningful in the cases of the gold-containing systems where we have established that total order exists within the chains.

To investigate whether there is any short-range interchain order in the gold-containing systems, $(M_{1/2}Au_{1/2})CN$, three different models were constructed (Figure 12), all of which incorporate the information on the structures of the individual ordered chains (i.e., $[Cu-NC-Au-CN-]_n$ and $[Ag-NC-Au-CN-]_n$) determined above. These models were chosen to investigate whether aurophilic bonding influences the arrangement of chains in the mixed gold-containing compounds and, hence, the structures adopted by these materials. Aurophilic bonding has previously been proposed as a reason for gold cyanide itself adopting the AuCN structure rather than the AgCN structure.[6]


dx.doi.org/10.1021/ja307087d | J. Am. Chem. Soc. 2012, 134, 16387−16400

Table 3. Structural Parameters (Bond Length, $r_{j-k}$/Å, Root-Mean-Square Variation in Bond Length, $u_{j-k}$/Å, and Coordination Number, $n_{j-k}$)[26] for the Neutron Correlation Functions of the Mixed-Metal and Parent Cyanides at 10 K

| | model | atom pair, $j-k$ | $r_{j-k}$/Å | $u_{j-k}$/Å | $n_{j-k}$ |
|---|---|---|---|---|---|
| $(Cu_{1/2}Au_{1/2})CN$ | Cu−NC−Au−CN−Cu− | C≡N | 1.1510(5) | 0.0360(8) | 0.962(8) |
| | | Cu−N | 1.825(1) | 0.047(1) | 1.92(2)[c] |
| | | Au−C | 1.977(2) | 0.046(2) | 1.92(2)[c] |
| $(Cu_{0.50}Ag_{0.50})CN$ | mixed model<br>85%: Cu−N and Ag−C<br>15%: Cu−C and Ag−N | C≡N | 1.1556(4) | 0.0378(6) | 0.955(6) |
| | | Cu−N | 1.8440(8)[a] | 0.0564(8)[c] | 1.66(2) |
| | | Cu−C | | | 0.304(3) |
| | | Ag−C | 2.069(2)[a] | 0.0564(8)[c] | 1.66(3) |
| | | Ag−N | | | 0.304(5) |
| $(Ag_{1/2}Au_{1/2})CN$ | Ag−NC−Au−CN−Ag− | C≡N | 1.1525(8) | 0.034(1) | 0.93(1) |
| | | Au−C | 1.981(3) | 0.047[b] | 1.82(3)[c] |
| | | Ag−N | 2.038(3) | 0.047[b] | 1.82(3)[c] |
| HT-CuCN[27] | Cu−N/C−Cu−C/N−Cu− | C≡N | 1.1537(1) | 0.0287(4) | |
| | | Cu−C | 1.8478(1)[a] | 0.0429(2) | |
| | | Cu−N | | | |
| AgCN[27] | Ag−N/C−Ag−C/N−Ag− | C≡N | 1.1552(1) | 0.0267(4) | |
| | | Ag−C | 2.0679(1)[a] | 0.0528(2) | |
| | | Ag−N | | | |
| AuCN[5] | Au−N/C−Au−C/N−Au− | C≡N | 1.1547(4) | 0.022(1) | |
| | | Au−C | 1.9717(5)[a] | 0.051(1) | |
| | | Au−N | | | |

[a]The M−N and M−C bond lengths are indistinguishable. [b]Fixed value. [c]Constrained value.

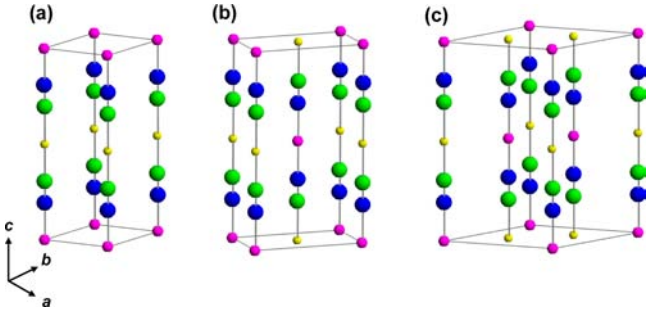


**Figure 12.** Three proposed models for the structure of $(Ag_{1/2}Au_{1/2})$-CN containing ordered $[Ag-NC-Au-CN-]_n$ chains in space group (a) *P6/mmm*[1], (b) *Immm*[2], and (c) *P6/mmm*[3]. [The number in brackets after the space group symbol corresponds to the number of $AgAu(CN)_2$ units in the unit cell.] Key: Au, yellow; Ag, pink; C, green; and N, blue. Similar models were used for $(Cu_{1/2}Au_{1/2})CN$.

Correlation functions, $T^N(r)_{model}$, were calculated over the range $r$ = 0−14 Å for the three $(Ag_{1/2}Au_{1/2})CN$ models and compared with the experimentally determined $T^N(r)$ function (Tables S.8−S.10, Figures S.11−S.13). The agreement for model (a) in *P6/mmm* is significantly worse than for models (b) and (c). This is surprising, as models (b) and (c) show reduced possibility for Au···Au aurophilic interactions compared to model (a): in (a), every Au atom has six Au near neighbors, whereas in (b) and (c), the average number of Au near neighbors is two. Models (b) and (c) differ in that (c) contains two crystallographically distinct Au atoms, one of multiplicity 2 with three Au neighbors and one of multiplicity 1 with no Au neighbors. A similar calculation for $(Cu_{1/2}Au_{1/2})CN$ (Tables S.11−S.13, Figures S.14−S.16) yielded no significant difference in the calculated $T^N(r)$ for each of the three models, showing that neutron diffraction is incapable of determining the nature of short-range interchain ordering in this compound. However, using evidence from the diffuse reflectance spectra below, we conclude that, in $(Cu_{1/2}Au_{1/2})CN$, the situation is similar to that found in $(Ag_{1/2}Au_{1/2})CN$. We emphasize that, if the interchain orderings of the types shown in (b) and (c) occur only over a short range and do not persist over the long range of a conventional crystallographic description, no superlattice reflections will appear in the Bragg diffraction pattern. This is in agreement with experiment. The long-range order can be destroyed by microtwinning of structures (b) and (c). It is remarkable that aurophilic interactions do not appear to be the driving force for the adoption of the gold cyanide structure by $(Cu_{1/2}Au_{1/2})CN$ and $(Ag_{1/2}Au_{1/2})CN$.

**Physical Properties.** *Thermal Expansion Behavior.* To investigate the thermal expansion behavior of the mixed-metal cyanides, their lattice parameters were measured between 95 and 490 K using PXRD. Thermal expansion coefficients, $\alpha_a$, $\alpha_c$, and $\alpha_{vol}$, were calculated over this temperature range and compared with data measured for the parent cyanides[9] (Table 4). An interesting feature of these materials and the parent cyanides is that they exhibit NTE along $c$ in the $[M-C\equiv N-]_n$ chain direction. This is accompanied by positive thermal expansion in the *ab* plane and an overall increase in cell volume. The relative percentage changes in the lattice parameters, $c$, as a function of temperature are shown in Figures 13 and 14. The changes in the corresponding $a$ lattice parameters and unit-cell volumes are shown in Figures S.17−S.19.

When comparing the thermal expansion coefficients of the parent cyanides, the value of $\alpha_c$ is much more negative for HT-CuCN and AgCN than for AuCN. It is notable that the mixed-


dx.doi.org/10.1021/ja307087d | J. Am. Chem. Soc. 2012, 134, 16387−16400

**Table 4. Thermal Expansion Coefficients, $\alpha$,[a] Determined between 95 and 490 K for Simple and Mixed Group 11 Metal Cyanides**

| | $\alpha_a/10^{-6}$ K$^{-1}$ | $\alpha_c/10^{-6}$ K$^{-1}$ | $\alpha_{vol}/10^{-6}$ K$^{-1}$ |
|---|---|---|---|
| HT-CuCN | 84.1 | −30.7 | 138.2 |
| AgCN | 70.8 | −24.8 | 117.4 |
| AuCN | 61.6 | −8.9 | 115.3 |
| $(Cu_{0.17}Ag_{0.83})CN$ | 73.9 | −26.0 | 122.5 |
| $(Cu_{0.33}Ag_{0.67})CN$ | 75.5 | −29.0 | 122.5 |
| $(Cu_{0.50}Ag_{0.50})CN$ | 75.8 | −34.5 | 117.2 |
| $(Cu_{0.67}Ag_{0.33})CN$ | 74.8 | −37.1 | 112.5 |
| $(Cu_{0.83}Ag_{0.17})CN$ | 78.3 | −40.1 | 116.5 |
| $(Cu_{2/3}Au_{1/3})CN$ | 86.5 | −15.0 | 160.0 |
| $(Cu_{1/2}Au_{1/2})CN$ | 83.3 | −13.8 | 154.6 |
| $(Ag_{1/2}Au_{1/2})CN$ | 83.9 | −9.0 | 161.0 |

[a]Coefficient of thermal expansion, $\alpha$, for a parameter $l$ is given by $\alpha_l = (l_T - l_0)/l_0(T - T_0)$, where $l_T$ is the parameter $l$ at temperature $T$ and $l_0$ is the parameter $l$ at the lowest temperature, $T_0$. $\alpha_a$ and $\alpha_c$ are the coefficients for the lattice parameters $a$ and $c$, respectively, while $\alpha_{vol}$ is the coefficient for the cell volume.

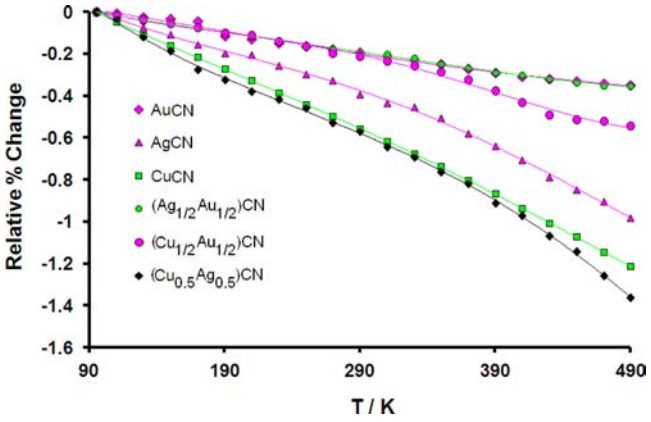


**Figure 13.** Relative percentage changes in the $c$ lattice parameters for $(Cu_{0.50}Ag_{0.50})CN$, $(Cu_{1/2}Au_{1/2})CN$, and $(Ag_{1/2}Au_{1/2})CN$ and the parent cyanides HT-CuCN, AgCN, and AuCN. The relative % change of a parameter, $l_T$, is given by $100 \times (l_T - l_0)/l_0$, where $l_T$ is the parameter $l$ at temperature $T$ and $l_0$ is the parameter $l$ at the lowest temperature, $T_0$.

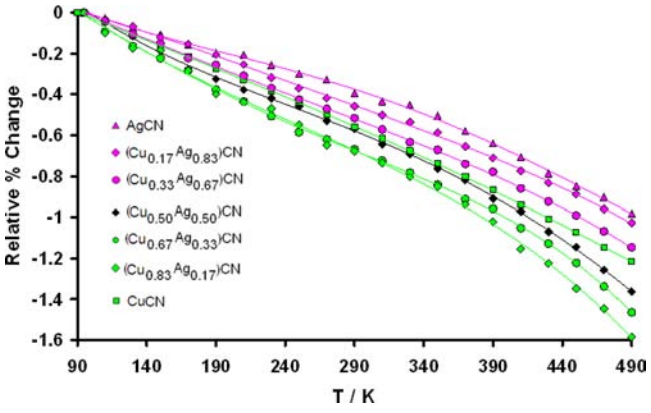


**Figure 14.** Relative percentage changes in the $c$ lattice parameter for AgCN, $(Cu_{0.17}Ag_{0.83})CN$, $(Cu_{0.33}Ag_{0.67})CN$, $(Cu_{0.50}Ag_{0.50})CN$, $(Cu_{0.67}Ag_{0.33})CN$, $(Cu_{0.83}Ag_{0.17})CN$, and HT-CuCN. The data are all fitted using fourth-order polynomials. The relative % change of a parameter, $l_T$, is given by $100 \times (l_T - l_0)/l_0$, where $l_T$ is the parameter $l$ at temperature $T$ and $l_0$ is the parameter $l$ at the lowest temperature, $T_0$.

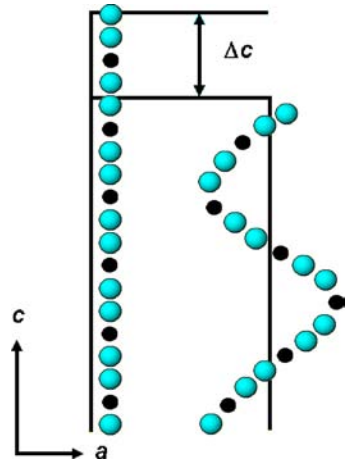


**Figure 15.** Thermal behavior of an $[M-(C/N)\equiv(N/C)-]_n$ chain. Key: metal, black; disordered cyanide groups, cyan. With increasing temperature, the $c$ lattice parameter contracts while the $a$ lattice parameter expands.

metal cyanides containing gold, i.e., $(Cu_{2/3}Au_{1/3})CN$, $(Cu_{1/2}Au_{1/2})CN$, and $(Ag_{1/2}Au_{1/2})CN$, have $\alpha_c$ values much closer to that of AuCN than to those of their other parent (Table 3). Indeed, below 300 K, the relative change in the $c$ parameter as a function of temperature for all the gold-containing phases is almost identical (Figure 13). For the AuCN-related compounds, structure type exerts more influence than composition over the NTE behavior.

Compounds adopting the AgCN structure type, i.e., those in the $(Cu_xAg_{1-x})CN$ system, together with the parents HT-CuCN and AgCN, show a larger NTE effect than the AuCN-related materials. In these materials, the composition has a bearing on the magnitude of the NTE. As $x$ increases from 0 to 0.83 in $(Cu_xAg_{1-x})CN$, the $\alpha_c$ value becomes steadily more negative (Table 3, Figure 14). Surprisingly, when $x = 1$, i.e., for HT-CuCN itself, the $\alpha_c$ value rises to a value in the middle of the range.

Lateral motions in the $ab$ plane normal to the chain direction, such as those the type shown in Figure 15, are known to contribute to the NTE effect in all these materials.[9] Such motions must be more constrained in the AuCN structure type than in the AgCN structure type. Lateral motions would be expected to force the chains apart, causing the expansion in the $ab$ plane, which is indeed observed to a similar degree for all materials (Table 3, Figures S.17−S.19).

*Diffuse Reflectance and Luminescence Spectroscopy.* Diffuse reflectance and luminescence spectra were collected for the mixed-metal cyanides $(Cu_xAg_{1-x})CN$, $(Cu_{1/2}Au_{1/2})CN$, and $(Ag_{1/2}Au_{1/2})CN$ and their parents CuCN, AgCN, and AuCN. It is noted that even the photophysical behavior of the parent cyanides is not fully understood. For example, although Bayse et al.[11,12] can explain some aspects of the photoluminescence behavior of LT-CuCN, AgCN, and AuCN, the energy-level diagrams are calculated only for isolated chain fragments rather than extended models. The fact that Bayse's calculations cannot account for the observed yellow color of AuCN shows that the description of these systems is incomplete. For the $(M_xM'_{1-x})CN$ materials, the aim is to determine whether they behave as physical mixtures of the simple parent cyanides, or if new optical behavior emerges.


dx.doi.org/10.1021/ja307087d | J. Am. Chem. Soc. 2012, 134, 16387−16400

Such new behavior may enable one type of metal−cyanide center within the chains to act as a sensitizer to promote emission from a different neighboring center and allow the tuning of optical properties by varying the metals and their compositions.

In the present work, diffuse reflectance spectra for the parents and mixed-metal cyanides are reported over the wavelength range 200−700 nm for the first time (Figure 16).

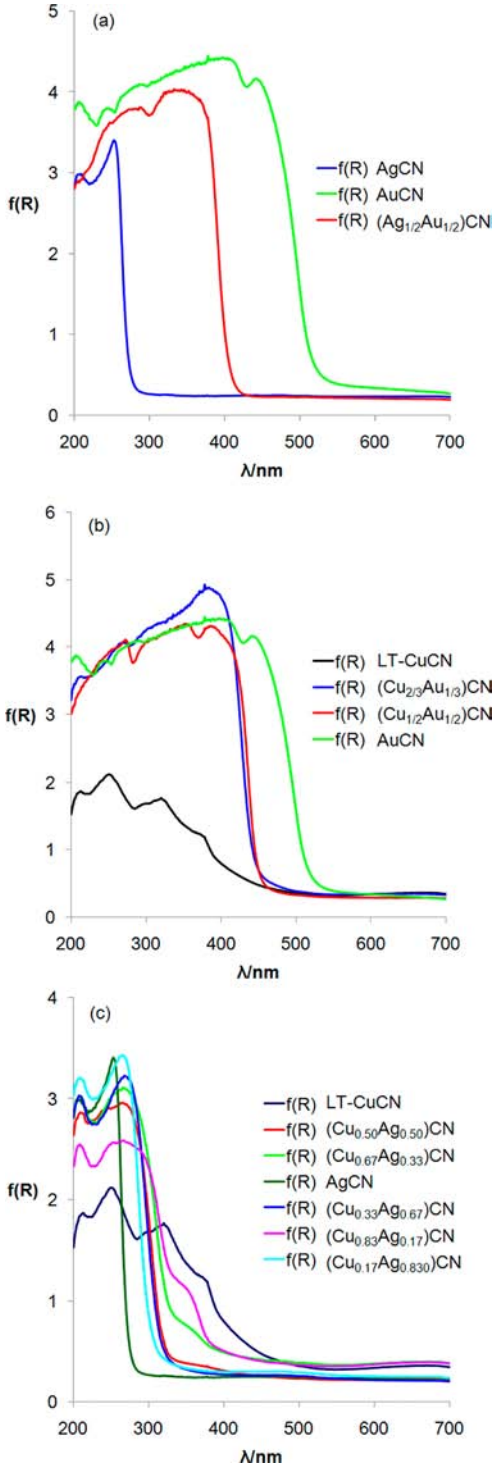


**Figure 16.** Diffuse reflectance spectra over the range 200−700 nm for the mixed-metal cyanides, $(M_xM'_{1-x})CN$, and their parents, LT-CuCN, AgCN, and AuCN.

All the gold-containing compounds absorb at the blue end of the visible region, explaining their yellow color, with AuCN being the most brightly colored (Table 1). The significant difference between the observed behavior for AuCN and that predicted by Bayse's model[12] must be due to interactions between gold−cyanide chains. We note that interactions between $[Au(CN)_2]^-$ ions in solution, ascribed to aurophilic bonding, cause a very large red shift in the absorption edge.[13,14] Bayse's calculations for isolated chain fragments, $(M_n(CN)_{n+1})^-$ (M = Cu, Ag),[11,12] agree more closely with the experimental absorption spectra for LT-CuCN and AgCN, suggesting that, in these cases, the interaction between chains does not have a major impact on the electronic energies in these systems and that they approximate to 1-D systems. In LT-CuCN, peaks are seen at 255, 300, 321, and 379 nm which can be assigned to the Laporte-allowed $\pi-\pi^*$ electronic transitions predicted by Bayse.[12] The absorption band edge observed in AgCN is at higher energy (lower wavelength) than in LT-CuCN (Figure 16c), also in agreement with the work of Bayse.[12]

The diffuse reflectance spectra of the mixed-metal cyanides show that, in all cases, the compounds do not behave merely as physical mixtures of the component parent cyanides. This is easiest to see in the gold cyanide-based systems, all of which have the AuCN structure. In the mixed silver−gold cyanide, $(Ag_{1/2}Au_{1/2})CN$, and the two mixed Cu−Au cyanides, $(Cu_{1/2}Au_{1/2})CN$ and $(Cu_{2/3}Au_{1/3})CN$, the spectra resemble most closely that of gold cyanide, but with the absorption edges shifted to higher energy (Figure 16a,b). In $(Ag_{1/2}Au_{1/2})CN$, this shift can be ascribed to a change in the interactions *between* rather than *within* the Ag−Au−cyanide chains. We have shown above that, in $(Ag_{1/2}Au_{1/2})CN$, the average number of gold atoms surrounding each gold atom within the metal sheets has fallen from six in AuCN to two (at ∼3.4 Å). We propose that a similar explanation applies in the cases of $(Cu_{1/2}Au_{1/2})CN$ and $(Cu_{2/3}Au_{1/3})CN$, which both have absorption edges close to that observed for $(Ag_{1/2}Au_{1/2})CN$. Unfortunately, using neutron diffraction, we were unable to determine local ordering within the metal sheets within $(Cu_{1/2}Au_{1/2})CN$.

The $(Cu_xAg_{1-x})CN$ series shows more complicated behavior (Figure 16c), which can be explained on the basis of the structural information obtained from vibrational spectroscopy and total neutron diffraction techniques. Thus, the distinct absorption edge seen around 325 nm for all the Cu−Ag cyanides can be ascribed to transitions between electronic states localized on copper−cyanide units bonded to silver atoms in the Ag−CN−Cu−NC−Ag unit. When $x$ exceeds 0.50 in $(Cu_xAg_{1-x})CN$, more extended copper−cyanide units, e.g., of the type Ag−CN−Cu−CN−Cu−NC−Ag, are formed in which copper atoms are no longer solely coordinated to the nitrogen end of the cyanide group. Thus, $(Cu_{0.67}Ag_{0.33})CN$ and $(Cu_{0.83}Ag_{0.17})CN$ behave like physical mixtures of $(Cu_{0.50}Ag_{0.50})CN$ and LT-CuCN. Close inspection of the high-wavelength end of the absorption edge of the diffuse reflectance spectrum for $(Cu_{0.50}Ag_{0.50})CN$ shows the presence of small portions of extended copper−cyanide chain, Cu−CN−Cu, within this compound. Evidence for such units in $(Cu_{0.50}Ag_{0.50})CN$ has been found in the Raman spectrum at ∼590 $cm^{-1}$.

With the exception of AgCN and $(Cu_{0.50}Ag_{0.50})CN$, the metal cyanides show significant absorption at a wavelength of 343 nm. This wavelength was subsequently used to excite photoluminescence. The luminescent behavior of the mixed-metal cyanides and their parents, including for the first time


dx.doi.org/10.1021/ja307087d | J. Am. Chem. Soc. 2012, 134, 16387−16400

**Table 5. Photophysical Properties of the Mixed-Metal Cyanides, $(M_xM'_{1-x})CN$, and Their Parents at 293 K[a]**

| | $\lambda_{exc}$/nm | $\lambda_{em}$/nm | Q.Y./% | $\tau_1$/ns | $\tau_2$/ns |
|---|---|---|---|---|---|
| $(Cu_{1/2}Au_{1/2})CN$ | 343 | 610 | – | 1.93 | 0.39[b] |
| | 350 | 610 | n.d. | – | – |
| | 420 | 610 | 0.7 | – | – |
| $(Cu_{2/3}Au_{1/3})CN$ | 343 | 440, 592 | – | 1.54 | 0.42[b] |
| | 420 | 592 | 0.3–0.4 | – | – |
| $(Ag_{1/2}Au_{1/2})CN$ | 343 | 420, 480 | – | 14.8 | 5.70 |
| | 385 | 420, 480 | 2.0–2.2[c] | – | – |
| | 405 | 480 | 1.25 | – | – |
| $(Cu_{0.50}Ag_{0.50})CN$ | 300 | ~520 | – | n.d. | n.d. |
| LT-CuCN | 343 | 398 | – | ~100[d] | ~0.3 |
| | 354[12] | 393 | n.d. | – | – |
| AgCN | 240[e] | 393, ~570 | n.d. | – | – |
| AuCN | 242[12] | 408, ~580 | n.d. | – | – |
| | 343 | 635 | – | 21 | 2.5 |
| | 515 | 635 | n.d. | – | – |

[a]In luminescence measurements, $\lambda_{exc}$ is the excitation wavelength (343 nm excitation obtained from laser, all other wavelengths from spectrofluorimeter), $\lambda_{em}$ is the maximum emission wavelength, Q.Y. is the quantum yield, and $\tau_1$ and $\tau_2$ are the lifetime components of the biexponential decay of luminescence. n.d. = not determined. [b]An additional long-lifetime component of the decay (~50 ns) is observed. [c]Q.Y. encompasses both 420- and 480-nm emissions. [d]The long-lived component of the luminescence decay could not be fitted accurately due to the weak signal and limitations of the instrument used. [e]AgCN emits only upon excitation with 240-nm light.[12]

information on luminescent lifetimes of LT-CuCN and AuCN, is summarized in Table 5. The red luminescence for $(Cu_{1/2}Au_{1/2})CN$ and blue luminescence for $(Cu_{2/3}Au_{1/3})CN$ and $(Ag_{1/2}Au_{1/2})CN$ are shown in Figures 17–19. The combined emission and excitation spectra for these materials are shown in Figures S.20–S.22, together with luminescence spectra for LT-CuCN and AuCN in Figures S.23 and Figure S.24.

All the mixed-metal cyanides studied using an excitation wavelength of 343 nm exhibit luminescence in the visible spectral region. $(Cu_{1/2}Au_{1/2})CN$ shows a red fluorescence response similar to that of AuCN, but with a slight shift to shorter wavelength (635 nm in AuCN compared to 610 nm in $(Cu_{1/2}Au_{1/2})CN$), suggesting that in both cases, a gold-based chromophore is involved. It is most likely that this is the NC–Au–CN unit, previously shown to be present in the mixed-metal material. $(Cu_{2/3}Au_{1/3})CN$ has a markedly different luminescence response spectrum compared to that of $(Cu_{1/2}Au_{1/2})CN$, showing a blue luminescence similar to that of LT-CuCN but shifted to slightly longer wavelength (440 nm compared to 398 nm), suggesting that the principal feature in the luminescence involves copper-based chromophores, such as Cu–CN–Cu. The very much weaker emission at 592 nm may, as above, arise from the NC–Au–CN units.

$(Ag_{1/2}Au_{1/2})CN$ produces blue luminescence on irradiation with 343 nm light. The parent cyanide AgCN does not even absorb at this wavelength, and AuCN emits in the red region. However, both AgCN and AuCN emit in the blue on excitation

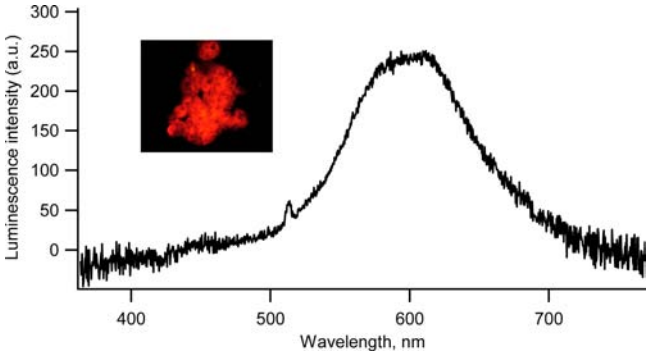


**Figure 17.** Red luminescence response of $(Cu_{1/2}Au_{1/2})CN$ to 343-nm laser light excitation showing $\lambda_{em}$ = 610 nm. Inset: luminescent image of microcrystals of $(Cu_{1/2}Au_{1/2})CN$.

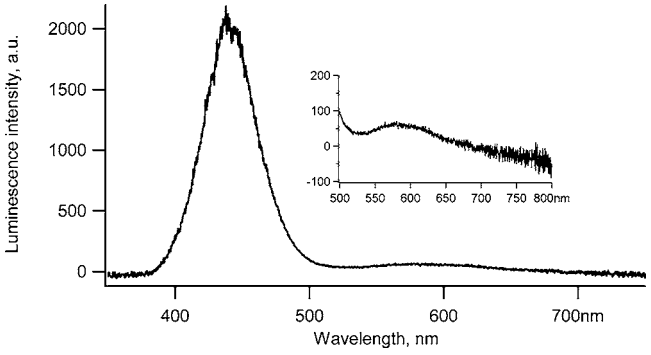


**Figure 18.** Blue luminescence response of $(Cu_{2/3}Au_{1/3})CN$ to 343-nm laser light excitation showing an intense emission with $\lambda_{em}$ = 440 nm and a weak emission with $\lambda_{em}$ = 592 nm (see inset).

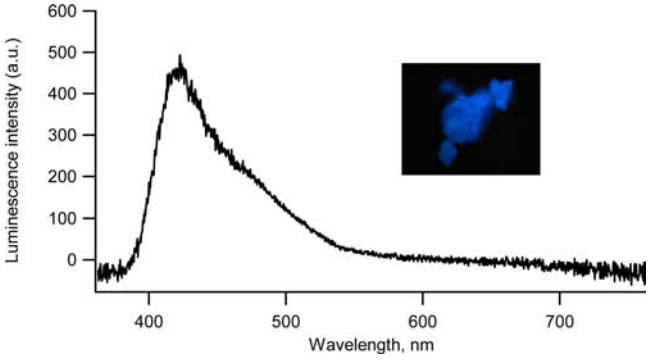


**Figure 19.** Blue luminescence response of $(Ag_{1/2}Au_{1/2})CN$ to 343-nm laser light excitation showing a composite emission with $\lambda_{em}$ = 420 and 480 (unresolved) nm. Inset: luminescent image of microcrystals of $(Ag_{1/2}Au_{1/2})CN$.

with 240 nm light.[12] In fact, the emission from $(Ag_{1/2}Au_{1/2})CN$ looks quite similar to that shown by Bayse for AgCN excited with 240 nm light,[12] with the exception that no band is seen at 580 nm for the mixed-metal compound. A plausible explanation is that the electronic structure of $(Ag_{1/2}Au_{1/2})CN$ allows access to the electronic states responsible for the photoemission of AgCN. This shows that by producing mixed-metal cyanides, we can tailor at least some of the photophysical properties.

To confirm our interpretation of the photophysical behavior of the Cu–Au cyanides and to gain some insight into the behavior of the Ag–Au cyanide, the nature of the states giving rise to luminescence will be analyzed in detail with DFT and TD-DFT and reported later. Previous DFT calculations on the


dx.doi.org/10.1021/ja307087d | J. Am. Chem. Soc. 2012, 134, 16387–16400

parent cyanides treated the metal−cyanide chains as isolated units,[11,12] but we have shown here that, particularly in the case of AuCN, this approach is far from satisfactory. The structural information determined in this work provides the basis necessary for construction of suitable models for the mixed-metal phases. However, dealing with the complexities of both inter- and intrachain disorder in extended solids is far from trivial.

## CONCLUSIONS

In this work, it has been demonstrated that mixed-metal cyanides of the group 11 metals can be prepared with general formula $(M_xM'_{1-x})CN$. In the copper−silver cyanide system, a solid solution, $(Cu_xAg_{1-x})CN$ $(0 \le x \le 1)$, is formed with the AgCN structure type. The gold-containing systems form the line phases, $(Cu_{1/2}Au_{1/2})CN$, $(Cu_{7/12}Au_{5/12})CN$, $(Cu_{2/3}Au_{1/3})$-CN, and $(Ag_{1/2}Au_{1/2})CN$, all with the AuCN structure.

In $(Cu_{1/2}Au_{1/2})CN$ and $(Ag_{1/2}Au_{1/2})CN$, both the metal atoms and cyanide groups are found using vibrational spectroscopy to be totally ordered within the chains. The sense of the ordering in $(Cu_{1/2}Au_{1/2})CN$ is unequivocally determined using total neutron diffraction to be $[Cu−NC−Au−CN−]_n$. We have also concluded, from neutron diffraction and by comparison with other systems, that in $(Ag_{1/2}Au_{1/2})CN$, the sense of cyanide bonding within the chains is $[Au−CN−Ag−NC−]_n$. In contrast, in $(Cu_{0.50}Ag_{0.50})CN$, metal ordering is incomplete, and strict alternation of metals does not occur along the chains. However, there is a distinct preference (85%) for the N end of the cyanide ligand to be bonded to copper and for Ag−CN−Cu links to predominate.

The thermal expansion behavior of these materials has been measured, and all compounds, like the simple parents HT-CuCN,[9] LT-CuCN,[3] AgCN,[9] and AuCN,[9] show negative thermal expansion along the direction of the metal−cyanide chains. All the gold-containing materials, including AuCN, show a smaller NTE effect compared to HT-CuCN, AgCN, and the copper−silver cyanides, showing the importance of structure over composition for this particular physical property. Future work will include a detailed study using total neutron diffraction, together with RMC modeling, to determine how the motions in the chains vary with structure type and composition. The photophysical properties of both parent and mixed-metal cyanides have been found to depend not only on the composition and order within individual chains but also on the structure type adopted. Interchain interactions were found to be extremely important in all compounds adopting the AuCN structure. The effect of composition on both thermal expansion and photophysical properties gives us the ability to tailor desirable properties in these mixed-metal cyanides.

It has been suggested that gold cyanide adopts the AuCN structure rather than the AgCN structure type because this results in much shorter interchain Au···Au distances and the opportunity for aurophilic interactions.[6] Such aurophilic interactions cannot, however, be the driving force in the adoption of the AuCN structure type by the gold-containing mixed-metal cyanides. Neutron diffraction shows that, in the case of $(Ag_{1/2}Au_{1/2})CN$, the local structure adopted appears to minimize the number of Au···Au interactions within the metal sheets formed on packing the chains together. In addition, diffuse reflectance spectroscopy shows that, although there are strong interchain interactions in $(Cu_{1/2}Au_{1/2})CN$, $(Cu_{2/3}Au_{1/3})CN$, and $(Ag_{1/2}Au_{1/2})CN$, the relative positions of the absorption edges can also be explained on the basis that the number of Au···Au interactions is minimized.

A forthcoming X-ray study of $(Cu_{1/2}Au_{1/2})CN$ will, because of the very different X-ray scattering factors of Cu and Au, provide definitive confirmation of interchain metal ordering in this compound.

## EXPERIMENTAL SECTION

Samples of $(Cu_xAg_{1-x})CN$, $(Cu_xAu_{1-x})CN$, and $(Ag_xAu_{1-x})CN$ were initially characterized using PXRD and IR and Raman spectroscopy. Room-temperature PXRD data were measured using a Siemens D5000 diffractometer (Cu K$\alpha$ radiation) operating in Bragg−Brentano geometry. IR and Raman spectra were collected from undiluted powders using a Perkin-Elmer Spectrum 100 FT-IR spectrometer with a Universal attenuated total reflection sampling accessory and a Renishaw InVia Raman microscope ($\lambda_{exc}$ = 785 nm), respectively. Atomic absorption measurements were made on samples of the $(Cu_xAg_{1-x})CN$ phases dissolved in dilute nitric acid and analyzed using a Perkin-Elmer 1100B atomic absorption spectrometer (Table S.2).

To measure the thermal expansion properties, PXRD patterns were collected at temperature intervals of 20 K using a Gemini S Ultra CCD diffractometer (high-intensity Enhance Ultra Cu K$\alpha$ radiation source) fitted with an Oxford Diffraction Cryojet HT (90−490 K). Samples were prepared by mixing ∼1 mg of a finely ground mixed-metal cyanide with silicon (internal calibrant) and mounted on a glass fiber using cyanoacrylate glue. Each X-ray diffraction image was collected for 240 s with a 360° rotation around $\varphi$ over the range $8 \le 2\theta/° \le 72$. Lattice parameters were determined from the positions of the first two sample peaks in the diffraction patterns, which correspond to the (101) and (110) reflections for the $(Cu_xAg_{1-x})CN$ phases and the (100) and (001) reflections for the gold-containing phases, respectively. Densities were measured at room temperature using a Quantachrome Micropycnometer with helium as the working gas (Table S.6).

**Sample Preparation.** ***Caution!*** *Cyanide materials are toxic and must be handled with care. The addition of acid to soluble cyanides liberates highly toxic gaseous HCN. Both gaseous HCN and the aqueous washings, which contain HCN, were destroyed using alkaline hypochlorite.*

Two methods were used for the synthesis of the mixed-metal group 11 cyanides, $(M_xM'_{1-x})CN$. The more general method, used to explore the full range of the CuCN−AgCN, CuCN−AuCN, and AgCN−AuCN cyanide systems, involved their precipitation by addition of acid to solutions of the parent cyanides in aqueous sodium or potassium cyanide (Tables S.1−S.5). A second method, specific to the composition $(Ag_{1/2}Au_{1/2})CN$, involved the addition of $Ag^+$ ions to a solution containing $[Au(CN)_2]^-$.

*Preparation of $(M_xM'_{1-x})CN$ Compounds by Acidification of Cyanide Solutions.* Aqueous solutions containing the $[Cu(CN)_4]^{3-}$, $[Ag(CN)_2]^-$, and $[Au(CN)_2]^-$ ions were prepared by dissolving the corresponding metal cyanides (LT-CuCN, AgCN, and AuCN) in a slight excess of KCN or NaCN. In order to explore the CuCN−AgCN, CuCN−AuCN, and AgCN−AuCN phases, solutions containing two of the metals were then mixed in various ratios. The mixed-metal cyanide compounds were then precipitated from solution by rapidly adding 2 M nitric acid in slight excess relative to the alkali-metal cyanide. All acid additions were performed under flowing nitrogen, and all exhaust gases from the experiments passed though a trap containing alkaline hypochlorite. The insoluble mixed-metal cyanide products were then filtered and washed well with water and dried in air. In the $(Cu_xAg_{1-x})CN$ system, samples with $x \ge 0.93$, formed initially with the LT-CuCN structure, were heated at 320 °C under vacuum for 2 h to convert them to the HT-CuCN (AgCN) structure. The above method was modified slightly for the preparation of gram-scale samples of $(Cu_{0.50}Ag_{0.50})CN$ and $(Cu_{1/2}Au_{1/2})CN$ required for the total neutron diffraction studies (Table S.6).

*Preparation of $(Ag_{1/2}Au_{1/2})CN$ by Reaction of $[Au(CN)_2]^-$ and $Ag^+$ Ions.* Attempts to make $(Ag_{1/2}Au_{1/2})CN$ via the acid addition method described above resulted in the formation of $(Ag_{1/2}Au_{1/2})CN$


dx.doi.org/10.1021/ja307087d | J. Am. Chem. Soc. 2012, 134, 16387−16400

contaminated with significant amounts of AgCN, which was easily identified by PXRD. A pure sample of $(Ag_{1/2}Au_{1/2})CN$ was, however, prepared by addition of $Ag^+$ ions to a solution of $[Au(CN)_2]^-$ in a 1:1 ratio. A silver nitrate solution, prepared by dissolving $AgNO_3$ (1.2 g, 7 mmol) in 50 mL of water, was added to a rapidly stirred $[Au(CN)_2]^-$ solution, prepared by dissolving gold cyanide (1.59 g, 7 mmol) in potassium cyanide (0.46 g, 7 mmol) in 50 mL of water. An off-white precipitate was immediately produced on mixing the two solutions. After a further 10 min of stirring, the solid was filtered, rinsed well with water, and allowed to air-dry. The method scaled up readily for the preparation of the larger sample of $(Ag_{1/2}Au_{1/2})CN$ used in the total neutron diffraction studies (Table S.6).

**Neutron Diffraction Experiments.** Time-of-flight powder neutron diffraction intensities were measured at 10 K for $(Cu_{0.50}Ag_{0.50})CN$ (0.7710 g), $(Cu_{1/2}Au_{1/2})CN$ (1.8100 g), and $(Ag_{1/2}Au_{1/2})CN$ (1.3646 g) on the GEM diffractometer[30] at the ISIS Facility, Rutherford Appleton Laboratory, Chilton, Didcot, UK. Samples were loaded into cylindrical 6 mm diameter thin-walled vanadium cans (of 25 $\mu$m thickness) so as to minimize the container background and absorption. The packing density of the sample, as used in the data correction routines, was determined from the sample depth and the can diameter. Background runs were collected on the empty can, CCR, and spectrometer, and absolute normalization data were collected for a standard vanadium rod.

The total neutron diffraction data were obtained from four detector banks (banks 2, 3, 4, and 5 at average scattering angles of 17.3, 34.3, 61.7, and 91.8°). Correction for multiple scattering, attenuation, and inelasticity and normalization to absolute scattering units was performed using the ATLAS[31] and GUDRUN[32] suites of programs (see Supporting Information). The corrected and normalized data from the four detector banks were merged in each case to yield an interference function, $Qi^N(Q)$, which covered the range $Q$ = 0.8−50 Å$^{-1}$, and this was then extrapolated to $Q$ = 0 Å$^{-1}$ (Figure S.9). The total correlation function, $T^N(r)$, is obtained by Fourier transformation of the interference function, $Qi^N(Q)$ (Figures S.11−S.17).

**Luminescence and Diffuse Reflectance Measurements.** Luminescence spectra, excitation spectra, and luminescence quantum yields were obtained using a Horiba Jobin-Yvon Fluorolog-3 spectrofluorimeter equipped with an F3018 integrating sphere of diameter 102 mm. The well-ground polycrystalline samples were coated onto the walls of a quartz cuvette. In addition, luminescence spectra and images, together with luminescence lifetimes, were measured on an inverted Nikon Eclipse TE2000U microscope, using a ×10:1.5 objective lens. The luminescence spectra were measured using an excitation wavelength, $\lambda_{exc}$ = 343 nm, obtained by taking the third harmonic generation output from a bismuth barium oxide (BBO) crystal illuminated by a TPulse200 ytterbium laser of wavelength $\lambda$ = 1030 nm with a pulse width of 407 fs, pulse frequency of 10 MHz, and energy of 260 nJ pulse$^{-1}$. Luminescence images and spectra of the microcrystals were obtained using an Ocean Optics Inc. spectrophotometer and a Nikon digital camera. Luminescence lifetimes were measured using a Europhoton Gmbh Quadrant Anode space- and time-correlated photon-counting photomultiplier mounted onto the microscope. Fluorescence lifetime imaging microscopy (FLIM measurements), determined for a number of crystallites in each sample using the photomultiplier, confirmed the homogeneity of the materials.

Diffuse reflectance spectra were measured by scanning over the wavelength range 200−2500 nm using a Perkin-Elmer Lambda 900 spectrophotometer equipped with an integrating sphere of 60 mm inner diameter. The polycrystalline samples, 1 mm in thickness, were held behind a quartz window. Absorption spectra were measured in terms of the Kubelka−Munk function ($f(R)$).[33]

## ■ ASSOCIATED CONTENT

### Supporting Information

Further details of the syntheses of the $(M_xM'_{1-x})CN$ phases and additional PXRD and thermal expansion data, vibrational spectra, diffuse reflectance and luminescence spectra, atomic absorption data for the $(Cu_xAg'_{1-x})CN$ phases, and details of total neutron scattering analysis for $(Cu_{0.50}Ag_{0.50})CN$, $(Cu_{1/2}Au_{1/2})CN$, and $(Ag_{1/2}Au_{1/2})CN$. This material is available free of charge via the Internet at http://pubs.acs.org.

## ■ AUTHOR INFORMATION


### Corresponding Author

a.m.chippindale@rdg.ac.uk; simon.hibble@stfc.ac.uk


### Notes

The authors declare no competing financial interest.

## ■ ACKNOWLEDGMENTS

The authors thank the EPSRC for a studentship for E.M. (Grant No. EP/G067279/1) and the EPSRC and STFC (via its Centre for Materials Physics and Chemistry Grant CMPC06101) for joint-funding of a studentship for E.J.B. The University of Reading is acknowledged for provision of the Chemical Analysis Facility (CAF). F.H. thanks Prof. Pierre Audebert and the ENS Cachan for supporting his visit to undertake luminescence measurements.

## ■ REFERENCES


(1) Hibble, S. J.; Hannon, A. C.; Cheyne, S. M.; Eversfield, S. G. *Inorg. Chem.* **2002**, *41*, 4990.
(2) Reckeweg, O.; Lind, A.; Simon, A.; DiSalvo, F. J. *Z. Naturforsch.* **2002**, *58b*, 155.
(3) Hibble, S. J.; Eversfield, S. G.; Cowley, A. R.; Chippindale, A. M. *Angew. Chem., Int. Ed.* **2004**, *43*, 628.
(4) Hibble, S. J.; Cheyne, S. M; Hannon, A. C.; Eversfield, S. G. *Inorg. Chem.* **2002**, *41*, 1042.
(5) Hibble, S. J.; Hannon, A. C.; Cheyne, S. M. *Inorg. Chem.* **2003**, *42*, 4724.
(6) Pyykko, P. *Angew. Chem., Int. Ed.* **2004**, *43*, 4412.
(7) Kroeker, S.; Wasylishen, R. E.; Hanna, J. V. *J. Am. Chem. Soc.* **1999**, *121*, 1582.
(8) Bryce, D. L.; Wasylishen, R. E. *Inorg. Chem.* **2002**, *41*, 4131.
(9) Hibble, S. J.; Wood, G. B.; Bilbé, E. J.; Pohl, A. H.; Tucker, M. G.; Hannon, A. C.; Chippindale, A. M. *Z. Kristallogr.* **2010**, *225*, 457.
(10) Lim, M. J.; Murray, C. A.; Tronic, T. A.; deKrafft, K. E.; Ley, A. N.; deButts, J. C.; Pike, R. D.; Lu, H.; Patterson, H. H. *Inorg. Chem.* **2008**, *47*, 6931.
(11) Bayse, C. A.; Brewster, T. P.; Pike, R. D. *Inorg. Chem.* **2009**, *48*, 174.
(12) Bayse, C. A.; Ming, J. L.; Miller, K. M.; McCollough, S. M.; Pike, R. D. *Inorg. Chim. Acta* **2011**, *375*, 47.
(13) Rawasdeh-Omary, M. A.; Omary, M. A.; Patterson, H. H. *J. Am. Chem. Soc.* **2000**, *122*, 10371.
(14) Rawasdeh-Omary, M. A.; Omary, M. A.; Patterson, H. H.; Fackler, J. P. *J. Am. Chem. Soc.* **2001**, *123*, 11237.
(15) Stender, M.; White-Morris, R. L.; Olmstead, M. M.; Balch, A. L. *Inorg. Chem.* **2003**, *42*, 4504.
(16) Katz, M. J.; Ramnial, T.; Yu, H.-Z.; Leznoff, D. B. *J. Am. Chem. Soc.* **2008**, *130*, 10662.
(17) Colis, J. C. F.; Larochelle, C.; Fernandez, E. J.; Lopez-de-Luzuriaga, J. M.; Monge, M.; Laguna, A.; Tripp, C.; Patterson, H. *J. Phys. Chem.* **2005**, *B109*, 4317.
(18) Chadwick, B. M.; Frankiss, S. G. *J. Mol. Struct.* **1976**, *31*, 1.
(19) Stammreich, H.; Chadwick, B. M.; Frankiss, S. G. *J. Mol. Struct.* **1968**, *1*, 191.
(20) West, A.R. *Solid State Chemistry and Its Applications*, 1st ed.; J. Wiley and Sons, Ltd.: New York, 1984; pp 366−369.
(21) Bowmaker, G. A.; Kennedy, B. J.; Reid, J. C. *Inorg. Chem.* **1998**, *37*, 3968.
(22) Murray, C. A.; Bodoff, S. *J. Chem. Phys.* **1986**, *85*, 573.
(23) Billinge, S. J. L.; Kanatzidis, M. G. *Chem. Commun.* **2004**, 749.

(24) Hibble, S. J.; Hannon, A. C.; Fawcett, I. D. *J. Phys. Cond. Matter* **1999**, *11*, 9203.
(25) Sears, V. F. *Neutron News* **1992**, *3*, 26.
(26) Hannon, A. C.; Grimley, D. I.; Hulme, R. A.; Wright, A. C.; Sinclair, R. N. *J. Non-Cryst. Solids* **1994**, *177*, 299.
(27) Cheyne, S. M. Ph.D. Thesis, The University of Reading, 2004.
(28) Grimley, D. I.; Wright, A. C.; Sinclair, R. N. *J. Non-Cryst. Solids* **1990**, *119*, 49.
(29) Meng, W.; Clegg, J. K.; Nitschke, J. R. *Angew. Chem., Int. Ed* **2012**, *51*, 1881.
(30) Hannon, A. C. *Nucl. Instrum. Methods* **2005**, *A551*, 88.
(31) Hannon, A. C.; Howells, W. S.; Soper, A. K. In *Institute of Physics Conference Serieses*; Johnson, M. W., Ed.; IOP Publishing Ltd.: Bristol, UK, 1990; Vol. *107*, p 193.
(32) Soper, A. K. Rutherford Appleton Laboratory Technical Report RAL-TR-2011-013,2011.
(33) Kubelka, P.; Munk, F. *Z. Tech. Phys.* **1931**, *12*, 593.